# A study on the effect of CT imaging acquisition parameters on lung nodule image interpretation

Shirley J.Yu[1], Joseph S.Wantroba[2], Daniela S. Raicu[2], Jacob D. Furst[2], David S. Channin[3], Samuel G. Armato III[4]
[1]University of Southern California, [2]DePaul University, [3]Northwestern University, [4]University of Chicago

## Abstract

Most Computer-Aided Diagnosis (CAD) research studies are performed using a single type of Computer Tomography (CT) scanner and therefore, do not take into account the effect of differences in the imaging acquisition scanner parameters. In this paper, we present a study on the effect of the CT parameters on the low-level image features automatically extracted from CT images for lung nodule interpretation. The study is an extension of our previous study where we showed that image features can be used to predict semantic characteristics of lung nodules such as margin, lobulation, spiculation, and texture. Using the Lung Image Data Consortium (LIDC) dataset, we propose to integrate the imaging acquisition parameters with the low-level image features to generate classification models for the nodules' semantic characteristics. Our preliminary results identify seven CT parameters (convolution kernel, reconstruction diameter, exposure, nodule location along the z-axis, distance source to patient, slice thickness, and kVp) as influential in producing classification rules for the LIDC semantic characteristics. Further post-processing analysis, which included running box plots and binning of values, identified four CT parameters: distance source to patient, kVp, nodule location, and rescale intercept. The identification of these parameters will create the premises to normalize the image features across different scanners and, in the long run, generate automatic rules for lung nodules interpretation independently of the CT scanner types.

## 1. Introduction

Research studies on CAD systems often use data from a single CT scanner. However, CAD systems trained on one type of CT scanner may not apply to images from a different manufacturer's CT scanner. Our research investigates differences between CT scanners and the effect of CT parameters on low-level image features automatically extracted from CT lung images. This study is an extension of our previous work[1] on semantic mapping in which we developed classification models to semantically interpret lung nodules based on low-level image features. Semantic mapping is important in modeling the relationship between image features and radiologist-defined semantic characteristics to understand the diagnosis decision making process instead of just the final decision of malignant versus benign. In this paper, we investigate the robustness of the semantic mappings with respect to the different CT scanner parameters used for the acquisition of the LIDC dataset[3]. While there are several research studies on the influence of the imaging acquisition parameters with respect to nodule detection algorithms[2] , nodule volume estimations[4,5], and image quality[6,7], the study presented in this paper is unique by addressing the influence of the CT scanner parameters on the automatic interpretation of lung nodules.

## 2. Methods

### 2.1 Data Collection

The dataset consists of lung images provided by the NIH/NCI LIDC Consortium formed by five institutions. It contains 85 cases, out of which 60 cases have 149 distinct lung nodules with diameter larger than 3mm. The nodules are marked by up to four radiologists with respect to nine semantic characteristics: calcification, internal structure, lobulation, malignancy, margin, sphericity, speculation, subtlety, and texture. We do not consider calcification and internal structure because all the nodules are given the same ratings of 'no calcification' and 'soft tissue' respectively. Therefore, our methodology focuses on seven LIDC semantic characteristics, each one of them rated on a scale from 1 to 5.

In terms of the low-level image features used to encode the lung nodule image content, we use the 64 image features previously extracted in our work[1] and summarized in Table 1 as shape, size, intensity, and texture feature types. The features for each nodule are coupled with the imaging acquisition parameters found in the DICOM header of the corresponding nodule image. Given the large number of parameters (103) and the fact that many of them have missing

values (not all manufacturers record values for certain parameters), we reduced the number of parameters from 103 to 14 by eliminating parameters with missing values or those that are unique identifiers. Table Height was additionally eliminated because it contains unreasonable outlier values. Manufacturer and Manufacture Model Name were eliminated as confounding variables that prevent more subtle differences in other CT parameters from appearing. Because Exposure Time and X-ray Tube Current are captured in the Exposure attribute (defined as the product of Exposure Time and Tube Current), we decided, of these three attributes, to use only Exposure. Table 2 summarizes the list of parameters analyzed in this study.

We produced a new parameter called Z Nodule Location to represent the location of the nodule in the lung along the z-axis. For each patient case, we found the z-coordinates (equivalent to Image Position Patient 3 in the DICOM header) of the top most and bottom most images of each lung to calculate the length of each lung. This allowed us to divide the lung into five subsections and to bin the location of the nodules into these five subsections. Later in our post-processing analysis, to perform equal-size binning of all CT parameters, Z Nodule Location was binned by dividing the lung into 3 subsections. We were thus able to locate all 149 lung nodules along the z-axis respective to each other. Thus, we used 14 parameters as summarized in Table 2.

### 2.2 Semantic Mapping: Decision Tree Classifier

Once CT image acquisition parameters, low-level image features, and semantic characteristics are integrated for lung nodule representation, a decision tree (DT) classification approach is applied to predict each one of the seven semantic characteristics based on the 64 low-level image features and 14 CT acquisition parameters. For our input, we used the 149 nodules from the LIDC dataset encoded using 64 image features and 14 CT acquisition parameters. The output was decision rules. The specifications for the decision tree are described in Table 3. After running the initial set of decision trees, we performed post-processing analysis on our DT results by running box plots and binning variables with a wide range of data. Our methodology is summarized in Figure 1.

Table 1: Image features; SD stands for standard deviation, BG for background, and MRF for Markov Random Fields

| **Shape Features** | **Size Features** | **Intensity Features** | **Texture Features** |
|---|---|---|---|
| Circularity | Area | Minimum Intensity | 11 Haralick features |
| Roughness | Convex Area | Maximum Intensity | 24 Gabor features |
| Elongation | Perimeter | Mean Intensity | 5 MRF features |
| Compactness | Convex Perimeter | SD Intensity | |
| Eccentricity | Equivalent Diameter | Minimum Intensity BG | |
| Solidity | Major Axis Length | Maximum Intensity BG | |
| Extent | Minor Axis Length | Mean Intensity BG | |
| Radial Distance SD | | SD Intensity BG | |
| | | Intensity Difference | |

Table 2: Final list of CT parameters

| | |
|---|---|
| 1. Slice Thickness | 2. Pixel Spacing 1 |
| 3. kVp | 4. Pixel Spacing 2 |
| 5. Reconstruction Diameter | 6. Bits Stored |
| 7. Distance Source To Patient | 8. High Bit |
| 9. Exposure | 10. Pixel Representation |
| 11. Bit Depth | 12. Rescale Intercept |
| 13. Convolution Kernel | 14. Z Nodule Location |

Table 3: Specifications for Decision Tree

| | |
|---|---|
| Cross-validation | 10 folds |
| Growth Method | C&RT |
| Max. Tree Depth | 50 |
| Parent Node | 5 |
| Child Node | 2 |

Figure 1: Diagram of the proposed methodology

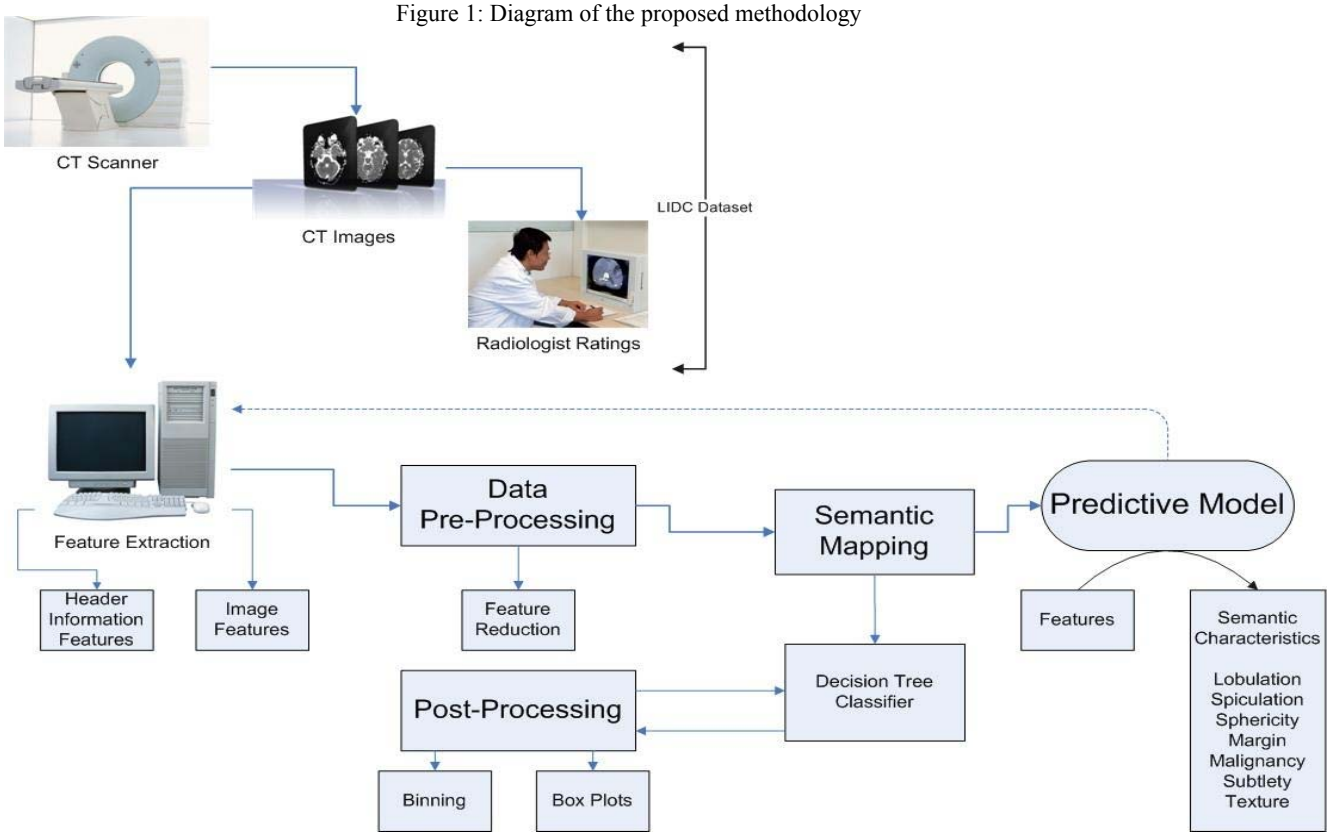


### 2.3 Post Processing: Box plots and Binning

When a predictor variable (i.e. a CT parameter or an image feature) appears in the DT, it splits a parent node into two child nodes. We are not only interested in how a predictor variable influences the prediction of the target variable (semantic characteristics in our case), but also how predictor variables influence each other within the decision tree. In our research, we analyzed the influence of CT parameters on image features. To perform this analysis, we ran box plots for image features appearing as a parent node directly above the CT parameter and image features appearing as child nodes directly below the CT parameter. This analysis allows us to determine if there are other differences due to image features between two child nodes besides the CT parameter. If our results show non-overlapping boxplots, this would indicate that the CT parameter is influential in how cases are sorted. In such instances, we would then try to eliminate the influence of the CT parameter by normalizing the image features using min-max normalization approach and normalizing the CT parameters using Z-transformation.

C&RT decision tree rules are influenced by the number of values for each predictor variable. If a variable has more values, it will more likely be selected in the decision rules. To minimize this influence, we performed equal-size binning so that all CT parameters have close to the same number of bins (i.e. 2 or 3 bins). For Convolution Kernel, which has categorical values, this parameter was binned based on kernel type: smoothing (value=1), edge-hardening (value =2), or neither (value =3). Our list of parameters was further reduced to 10 parameters due to redundant variables. Pixel spacing 2 was removed because it had values identical to Pixel Spacing 1. Bit Depth was found to have a correlation of 1 with High Bit, Bits Stored, and Pixel Representation. Due to redundancy, High Bit, Bits Stored, and Pixel Representation were removed. If parameters had 3 or less values (Distance Source to Patient, Bit Depth, and Rescale Intercept), they were not binned. Z-Nodule Location was re-binned into 3 bins (1=apex, 2=middle, and 3=base).

Of the remaining parameters, Reconstruction Diameter, Exposure, and Pixel Spacing 1 were all binned with 3 equal-width bins. Slice Thickness and kVp were binned into 3 bins by rounding the values to the nearest whole value in the case of Slice Thickness and the nearest ten in the case of kVp.

**Table 4:** Range of values for CT parameters after binning

| | Slice Thickness | kVp | Reconstruction Diameter | Distance Source to Patient | Exposure | Convolution Kernel | Pixel Spacing | Rescale Intercept | Bit Depth | Z Nodule Location |
|---|---|---|---|---|---|---|---|---|---|---|
| | 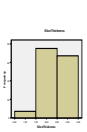 | 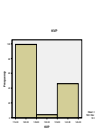 | 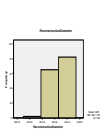 | 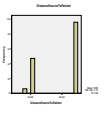 | 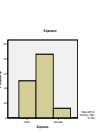 | 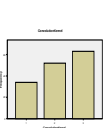 | 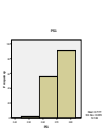 | 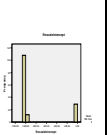 | 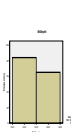 | 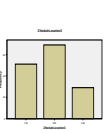 |
| Values | 1 | 120 | 260 | 535 | 25 | 1 (Smoothing) | .51 | -1024 | 12 | 1 (Apex) |
| | 2 | 130 | 330 | 541 | 1125 | 2 (Edge Enhancement) | .64 | -1000 | 16 | 2 (Middle) |
| | 3 | 140 | 400 | 570 | 2225 | 3 (Neither) | .77 | .00 | | 3 (Base) |

## 3. Results

### 3.1 Decision Tree Results

The DT classification approach predicted each of the seven characteristics with at least 85% accuracy based on low-level image features and CT parameters. We used SPSS Answer Tree to generate C&RT decision trees; Answer Tree uses a brute force to exhaustively examine all of the fields of the dataset with respect to the target variable (semantic characteristic) to find the "best" split. The best split can be defined by the improvement score (Table 4) in the information gain criterion. The CT parameters with higher improvement will appear higher up in the decision trees.

Table 5: Results from DT classification before any post-processing analysis, showing influential CT parameters and the semantic characteristics they predict for. The first value in parenthesis represents the improvement, and the second value represents the level at which the CT parameter appears in the decision tree.

| | Convolution Kernel | Reconstruction Diameter | Exposure | Distance Source to Patient | Z Nodule Location | kVp | Slice Thickness |
|---|---|---|---|---|---|---|---|
| Texture | (0.032, 3) | (0.018, 8) | - | - | - | - | - |
| Subtlety | (0.032, 3)<br>(0.014, 8) | - | (0.022, 6) | - | (0.017, 10) | - | - |
| Spiculation | - | - | (0.043, 2) | (0.016, 6) | - | - | (0.016, 9) |
| Sphericity | - | - | - | - | (0.019, 6) | (0.036, 3) | - |
| Margin | (0.020, 9) | (0.019, 10) | - | - | - | - | - |
| Malignancy | - | - | (0.015, 3) | - | (0.019, 6) | - | - |
| Lobulation | - | - | (0.052, 2) | (0.021, 6) | - | - | - |

*Convolution Kernel and Reconstruction Diameter* appear as predictors for texture and margin, two correlated characteristics (correlation= 0.62)[8]. Convolution Kernel additionally predicts for subtlety. Given the definitions of subtlety (the contrast between nodule and surrounding), margin (how well defined the nodule margins are), and texture (the internal density of the nodule), using one of the two general categories for convolution kernels (a soft kernel for smoothing and a sharp kernel for edge enhancement) would understandably affect nodule characteristics. Furthermore, our findings appear to be in agreement with literature review showing that the type of convolution kernel influences image features[2].

Though Convolution Kernel appears with high information gain in predicting texture and margin, the decision rules do not appear to sort cases based on the type of kernel (smoothing versus edge enhancement). We ran some further

analysis to investigate if Convolution Kernel influences other image features which are not evident from the decision tree. In our post-processing analysis, our boxplot results demonstrate that only Convolution Kernel is influential over image features, specifically the intensity features: MinIntensity, MaxIntensity, MeanIntensity, MinIntensity BG, MaxIntensityBG, and MeanIntensityBG (Figure 2). Images reconstructed with kernels FC01, D, and Bone have lower values for intensity features, and images reconstructed with B30f and Stan kernels have higher intensity values. Since Convolution Kernel also appears in the DT targeting Margin, we performed this same analysis for the Margin DT but found all the box plots of image features had overlapping values. These results suggest that Convolution Kernel affects semantic predicting of texture by influencing intensity features. However, later post-processing analysis show that the effect of Convolution Kernel can be eliminated by proper binning.

We first tried to eliminate the influence of Convolution Kernel by normalizing the image features. However, Convolution Kernel continued to appear in the decision tree even after normalization. Convolution Kernel was successfully eliminated by binning the values by kernel type as either smoothing, edge enhancement, or neither. Thus the type of kernel (as smooth, edge, or neither) used for image reconstruction does not influence semantic predicting. We suspect there may be other confounding properties of Convolution Kernel that the manufacturers have kept private.

Figure 2: Box plots of intensity features split based on type of Convolution Kernel

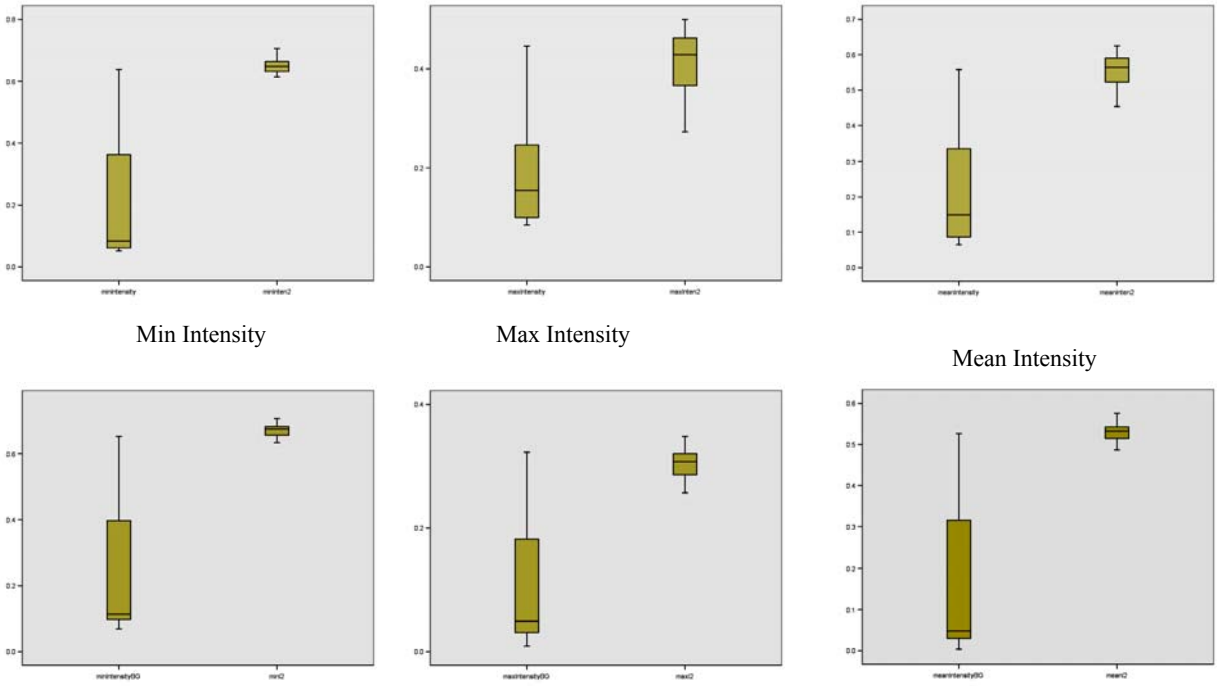

Min Intensity | Max Intensity | Mean Intensity

Min IntensityBG | Max IntensityBG | Mean IntensityBG

*Reconstruction Diameter* is defined as the diameter of the region used to reconstruct the image. Also known as Field of View, this parameter is essentially equal to the product of Pixel Spacing and 512. When unbinned, Reconstruction Diameter appears together with Convolution Kernel in the decision tree. We conclude that parameters affecting the reconstruction of CT images influence prediction of texture and margin. Our results indicate that a reconstruction diameter less than 382.031 (from a range of 260-390mm in our data) sorts 20 out of the 22 given nodules (from the parent node) as a solid texture (c=5) with 100% accuracy. However, when binned, Reconstruction Diameter fails to appear in the decision trees.

*Exposure and kVp* represent two properties of the x-ray beam: beam quality, or the ability of the beam to penetrate an object (controlled by *kVp*), and beam intensity, or number of x-ray photons in the beam (controlled by Exposure). In our results, kVp appears in the decision tree targeting sphericity, while Exposure appears for subtlety, spiculation, malignancy, and lobulation. The frequency of Exposure appearing in our semantic predicting compared to kVp can be explained by the fact that kVp settings are not usually modified in CT scanning[10]. In our dataset, Exposure has a wider range of values than kVp.

*Exposure and Distance Source to Patient* appear as predictors for two correlated semantic characteristics: spiculation and lobulation (correlation = 0.65)[8]. For both characteristics, Exposure appears with the highest information gain in the tree (improvement = 0.043 and 0.0524 for spiculation and lobulation respectively). Cases with an Exposure > 890 mAs predict with 79.31% accuracy no lobulation (c=5, 4), and cases ≤ 890 mAs are predicted with 56.57% accuracy to be markedly lobular (c = 1,2). Cases with Exposure >= 910 mAs are predicted with 64.28% accuracy to be little spiculated (c=5,4), and cases at less than 910 mAs have a 71.90% accuracy of being highly spiculated (c= 1,2). It appears a higher Exposure causes a less lobulated and spiculated appearance of the nodule.

*Distance Source to Patient* is defined as the distance between x-ray beam source and the patient; the square of Distance Source to Patient is inversely proportional to Exposure [10, 11]. We performed a correlation on the LIDC dataset to confirm the relationship between these two parameters and found a correlation= -0.704.

When equal-size binning was performed, Exposure was eliminated, and when predicting lobulation, Distance Source to Patient replaced Exposure as having the highest information gain. A higher value for Distance Source to Patient (570) predicts with 61% accuracy a more lobular shape (c1, c2); a lower value (541, 535) predicts with 41% accuracy no lobulation (c5). The fact that Distance Source to Patient appears after equal-size binning but not Exposure is reasonable given how decision trees run. If two predictor variables are similar, C&RT decision trees use the predictor variable with higher information gain. Since Distance Source to Patient and Exposure are inversely correlated, we can reasonably expect the decision tree to use only one of the two parameters in the decision rules.

*Z Nodule Location* is the only parameter in this experiment not extracted from a DICOM header. This parameter identifies the location of a nodule in the lung along the z-axis. A value of 1 means the nodule is in the lung apex, and a value of 5 indicates the nodule is in the lung base. The appearance of this parameter in prediction for subtlety, sphericity, and malignancy suggests that whether a nodule is located in the apex or base of the lung affects predicting for these semantic characteristics.

*Slice Thickness* appeared in the decision tree targeting spiculation as a leaf node. Our literature review suggests Slice Thickness is important in spatial resolution (thinner slices result in higher spatial resolution)[11]. However, the appearance of Slice Thickness as a leaf node with low information gain, and its disappearance after binning, suggests this CT parameter is not significant in our semantic predicting.

*Rescale Intercept*, having only three values, was not binned. However, binning of other values allows this parameter to appear in the decision tree. Along with Rescale Slope, this parameter specifies the relationship between CT values measured in Hounsfield Units (HU) and the values encoded in pixel format (called "stored values"). The relationship is defined as:

CT values = m*SV + b, where m = Rescale Slope, SV = stored values, and b = Rescale Intercept[9].

**Table 5**: CT parameters appearing in decision trees after equal-size binning

| | Z Nodule Location | Distance Source to Patient | KVP | Rescale Intercept |
|---|---|---|---|---|
| Texture | | | | |
| Subtlety | **X** | | | **X** |
| Spiculation | **X** | **X** | | |
| Sphericty | | | **X** | |
| Margin | | | | |

| | | | | |
|---|---|---|---|---|
| Malignancy | | | | |
| Lobulation | | **X** | | |

### 3.2 Results: Box plots

**Table 6:** Image features appearing as child nodes directly under CT parameters

| **CT Parameters** | **Image Features** |
|---|---|
| *Convolution Kernel* (B30f, B31f, B31s, Bone, C, D, FC01 , Stan) | Gabor, Inverse Variance, Major Axis Length, Elongation, Compactness |
| *Reconstruction Diameter* (260-390 mm) | Markov |
| *Exposure* (25-2108 mAs) | Gabor, Minimum Intensity, Circularity, Homogeneity, Compactness |
| *kVp*(120, 130, 135, 140) | Elongation, Perimeter |
| *Z Nodule Location* (1-5; 1= lung apex, 5 = lung base) | Radial Distance, Minimum Intensity |
| *Distance Source to Patient* (535, 541, and 570 mm) | Contrast, Gabor |

The image features having a CT parameter as a parent node was identified as being dependent on the CT parameter for the corresponding semantic characteristic. Table 6 summarizes image features with the highest probability to be dependent on the CT parameters. To determine more precisely how these image features are being influenced by CT parameters, box plots on image features were run comparing cases sorted by CT parameters into their respective child nodes.

Our results show that box plots comparing cases sorted into two child nodes based on CT parameter decision rules overlap for the same range of values. Only two box plot comparisons had non-overlapping graphs: a box plot of Radial Diameter split by Exposure when predicting Subtlety and a box plot of Third Order split by Z Nodule Location when predicting Sphericity (Table 7). Non-overlapping box plots would suggest that the image features plotted are influenced by the CT parameter. However, our results are not conclusive because the number of cases in each child node vary and can be as little as two. The child nodes split by Exposure in the Subtlety tree contain 8 and 3 cases. The child nodes split by Z Nodule Location in the Sphericity tree contain 2 and 13 cases. Thus, even though the box plots for Gabor are non-overlapping, the dataset is too small to be conclusive.

**Table 7**: Non-overlapping boxplots of image features comparing child nodes split by specified CT parameter when predicting specified semantic characteristic

| **Semantic Characteristic** | **CT parameter** | **Image Feature** |
|---|---|---|
| Subtlety | Exposure | Radial Diameter |
| Sphericity | Z Nodule Location | Third Order |

Since more than one leaf node contains only two cases, we hypothesized that when only two cases are sorted into a child node, representing 10% or less of the original number of cases in the parent node, these cases are outliers. Box plots were run comparing image features for "outlier" cases and the remaining cases. However, there were no distinctly separated box plots; all were overlapping.

## 4. Conclusion

While there are several research studies on the influence of the imaging acquisition parameters with respect to nodule detection algorithms, nodule volume estimations, and image quality, the study presented in this paper is unique by addressing the influence of these CT scanner parameters on the automatic interpretation of lung nodules based on low-level image features. Our preliminary results on 149 nodules identify seven CT parameters influential in producing

classification rules for the LIDC semantic characteristics: Convolution Kernel, Reconstruction Diameter, Z Nodule Location, Exposure, kVp, Distance Source to Patient, and Slice Thickness. Of these seven parameters, we found that correct binning eliminates Convolution Kernel, Reconstruction Diameter, Exposure, and Slice Thickness, and introduces a new parameter, Rescale Intercept. As future work, we plan to validate the results on more lung nodules as they become available from the LIDC consortium. The identification and validation of these parameters as being important will create the premises for normalizing image features across different scanners with the final goal of generating robust models for automatic lung nodule interpretation.

## 5. References

[1] Raicu DS, Varutbangkul E, Furst JD, Armato III SG. "Modeling semantics from image data: opportunities from LIDC". International Journal of Biomedical Engineering, Vol. 2, (3), 2009. (to appear)

[2] Armato, S G., M B. Altman, and P J. La Riviere. "Automated Detection of Lung Nodules in CT Scans: Effect of Image Reconstruction Algorithm." Medical Physics 30 (2003): 461-472.

[3] Horsthemke, W H., D S. Raicu, and J D. Furst. "Evaluation Challenges for Bridging Semantic Gap: Shape Disagreements on Pulmonary Nodules in the Lung Image Database Consortium." International Journal of Healthcare Information Systems and Informatics (IJHISI) Special Edition on Content-Based Medical Image Retrieval (2008).

[4] Way, TW, HP Chan, MM Goodsitt, et al. "Effect of CT Scanning Parameters on Volumetric Measurements of Pulmonary Nodules by 3D Active Contour Segmentation: a Phantom Study." Physics in Medicine and Biology 53 (2008): 1295-1312.

[5] Goo, JM., T. Tongdee, R. Tongdee, Kwangjae Yeo, CF. Hildebolt, and KT. Bae. "Volumetric Measurement of Synthetic Lung Nodules with Multi–Detector Row CT: Effect of Various Image Reconstruction Parameters and Segmentation Thresholds on Measurement Accuracy." Radiology 235 (2005): 850-856.

[6] Zerhouni, EA., JF. Spivey, RH. Morgan, FP. Leo, FP. Stitik, and S S. Siegelman. "Factors Influencing Quantitative CT Measurements of Solitary Pulmonary Nodules." J Comput Assist Tomogr 6 (1982): 1075-1087.

[7] Birnbaum, B, N Hindman, J Lee, and J Babb. "Multi-Detector Row CT Attentuation Measurements: Assessment of Intra- and Interscanner Variability with an Anthropomorphic Body CT Phantom." Radiology 242 (2007): 110-119.

[8] Raicu, DS., E. Varutbangkul, JG. Cisneros, JD. Furst, DS. Channin, SG. Armato III. "Semantics and image content integration for pulmonary nodule interpretation in thoracic computed tomography." The 7th IEE ICDM '07 Workshop on Data Mining (2007).

[9] Association National Electrical Manufacturers: Digital Imaging and Communication in Medicine (DICOM), part 3: Information Object Definitions. In, Rosslyn, VA: NEMA, 2008. Available at: http://medical.nema.org/dicom/2008/08_03pu.pdf. Last accessed August 7, 2008

[10] YS Cordoliani, V Hazebroucq, JL Sarrazin, C Leveque, B Vincent, E Jouan. "Helical Computed Tomography: Patient Exposure and Appropriate Use." Journal de Radiologie 80 (2008): 903-911.

[11] Dalrymple, NC, SR Prasad, MW Freckleton, KN Chintapalli. "Informatics in Radiology: Introduction to the Language of Three-Dimensional Imaging with Multidetector CT." Radiographics 25 (2005):1409-1428.